

**Coronal density diagnostics with Si X: CHANDRA/LETGS
observations of Procyon, α Cen A&B, Capella and ϵ Eri**

G. Y. Liang, G. Zhao, and J. R. Shi

National Astronomical Observatories, Chinese Academy of Sciences,
Beijing 100012, P. R. China

gzhao@bao.ac.cn

Received _____; accepted _____

ABSTRACT

Electron density diagnostics based on a line intensity ratio of Si X are applied to the X-ray spectra of Procyon, α Cen A&B, Capella and ϵ Eri measured with the Low Energy Transmission Grating Spectrometer (LETGS) combined with High-resolution Camera (HRC) on board the *Chandra X-ray Observatory*. The ratio R_1 of the intensities of the Si X lines at 50.524 Å and 50.691 Å is adopted. A certain of the temperature effect in R_1 appears near the low-density limit region, which is due to the contamination of Si X line at 50.703 Å. Using the emission measure distribution (EMD) model derived by Audard et al. (2001) for Capella and emissivities calculated with APEC model by Smith et al. (2001), we successfully estimate contributions of Fe XVI lines at 50.367 Å and 50.576 Å (73% and 62%, respectively). A comparison between observed ratios and theoretical predictions constrains the electron densities (in logarithmic) for Procyon to be $8.61_{-0.20}^{+0.24}$ cm $^{-3}$, while for α Cen A&B, Capella and ϵ Eri to be $8.81_{-0.23}^{+0.27}$ cm $^{-3}$, $8.60_{0.32}^{+0.39}$ cm $^{-3}$, $9.30_{-0.48}$ cm $^{-3}$ and $9.11_{-0.38}^{+1.40}$ cm $^{-3}$, respectively. The comparison of our results with those constrained by the triplet of He-like carbon shows a good agreement. For normal stars, our results display a narrow uncertainty, while for active stars, a relatively larger uncertainty, due to the contamination from Fe XVI lines, is found. Another possible reason may be that the determination of the continuum level, since the emission lines of Si X become weak for the active stars. For ϵ Eri, an electron density in the C V forming region was estimated firstly through Si X emissions.

Subject headings: line : identification – stars: late-type – stars : coroneae – X-rays : stars

1. Introduction

Since the seminal work by Vaiana et al. (1981), it has become clear that all late-type stars share the same basic coronal characteristics: hot thermal plasma with temperatures around 1–10 MK covering stellar surfaces, magnetic confinement, the presence of flares, etc. A systemic investigation indicates that most active stars have X-ray luminosity up to 2 orders of magnitude higher than that of solar corona (Scelsi et al. 2005; Peres et al. 2004). Present popular assumption for interpretation of such difference can be attributed to their different composition in terms of various kinds of coronal structures (ranging from the relatively faint and cool structures of the background corona to the very bright and hot flaring regions) and to the number of X-ray emitting coronal structures present.

The solar corona as observed with the modern X-ray and XUV telescopes on board Yohkoh, SoHO, or TRACE, is found to be extremely structured, and even in the high angular resolution TRACE images, it appears to be spatially unresolved fine structure. Yet spatially resolved X-ray observations of stellar coronae are currently not feasible. Some information on the spatial distribution of stellar coronae was inferred from X-ray light curves of suitably chosen stars such as eclipsing binaries (White et al. 1990; Schmitt & Kürster 1993; Güdel et al. 1995, 2003; Siarkowski et al. 1996), but such analyses can only be carried out for very special systems with advantageous geometries, and the actual information derivable from such data is rather limited. Another method to infer the structure in spatially unresolved data is spectroscopic measurements of the electron density, that is, X-ray spectra allow us to get the structure information for a various stellar coronae. Nevertheless, the temperature distribution (or emission measure distribution EMD) and the coronal abundance could be estimated from low-resolution spectra by an application of global fitting approaches. While the previous measurements did not allow measuring density n_e and emission measure EM independently because the information from spectral

lines was not available from spectra with the low resolution, such that no emitting volumes V could be estimated from $EM = n_e^2 V$. Therefore the information about loop size wasn't accessible.

Direct spectroscopic information on plasma densities at coronal temperatures on stars other than the Sun firstly became possible with the advent of “high-resolution” spectra ($\lambda/\Delta\lambda \sim 200$) obtained by the *Extreme Ultraviolet Explorer* (EUVE) which is capable of separating individual spectral lines. Even with this resolution, the available diagnostics have often tended to be not definitive, owing to the poor signal-to-noise ratio (SNR) of the observed spectra or blended lines. After the launch of new generation satellites *Chandra* and *XMM-Newton*, the high-resolution spectra coupled with the large effective area has made it is possible to measure individual lines in the X-ray range for a large sample of stars in the same fashion as X-ray emission lines from the solar corona obtained and analyzed for many years (Doyle 1980; McKenzie & Landecker 1982; Gabriel et al. 1988). The emissivity of selected lines depends on the density. Some lines may be present only in low-density plasmas, such as the forbidden line in He-like triplet, while other lines may appear only in high-density plasmas (such as lines formed following excitations from excited levels).

Ness et al. (2002, 2004) systemically investigated the coronal density using the characteristic of He-like triplet for stars with various activity covering inactive and active levels. For the hot-temperature region, the density is estimated from emission lines of carbon-like iron, and a typical density ranging 10^{11} – 10^{12}cm^{-3} was obtained. For the low-temperature region, the density can be derived from low- Z elements with low ionization energies such as C V, which is lower by at least an order of magnitude than that of the hot-temperature region. A typical electron density ranging 10^8 – 10^{10}cm^{-3} has been derived for solar and solar-like coronae by authors (Audard et al. 2001, Brinkmann et al. 2000). In inactive stars, emission lines of Si VII–Si XIII have also been clearly detected, and

some lines of Si X show a high SNR in the wavelength range covered by LETGS. In the collision ionization equilibrium (Mazzatto et al. 1998) condition, the temperature of peak fractional abundance of Si X is very close to that of C V. This means that they form in the same region and share the same electron density. Therefore, the density derived from Si X should be comparable to that from He-like C V. In our recent work (Liang et al. 2005), we noticed that the line intensity ratio R_1 of Si X at the lines at 50.524 Å and 50.691 Å originating from $3d \rightarrow 2p$ transitions is sensitive to the density, whereas it is insensitive to the temperature. So an application of this ratio R_1 in several stellar coronal spectra is performed.

In this paper, we derive the electron densities for stars: Procyon, α Cen A&B, Capella and ϵ Eri using this ratio R_1 for the first time, and compare the derived densities with those from He-like C V. The paper is structured as follows: we present our sample and a detailed description of line flux measurements in Sect. 2. A brief description of theory model is introduced in Sect. 3. Diagnostic of the electron density and discussions are presented in Sect. 4. The conclusions are given in Sect. 5.

2. Observations and data analyses

The new generation of X-ray telescopes and X-ray spectrometers on board *Chandra* and *XMM-Newton* has opened the world of spectroscopy to the X-ray astronomy with high-resolution and high effective collecting areas. Spectroscopic measurements can be performed with instruments, such as the Reflection Grating Spectrometer (RGS) on board *XMM-Newton*, and the High and medium Energy Grating (HEG and MEG) spectrometers, and the Low Energy Transmission Grating Spectrometer (LETGS) on board *Chandra*. Though RGS, HEG, and MEG provide large effective areas in the high energy region (5 to 40 Å) with high-resolution, the LETGS covers a much larger wavelength range 5–175 Å

with the high spectral resolution. One specific advantage of the LETGS resulting from its covered large range of wavelength is that the O VII triplet at around 21 Å, the C V triplet at around 41 Å and $3d \rightarrow 2p$ transition lines at 50 Å of Si X can be measured in one spectrum. In this wavelength range, a number of emission lines from highly ionized Si ions have been found in the coronal spectra (Raassen et al. 2002, 2003). Here, we pay a special attention on the emission lines at 50.524 Å and 50.691 Å of Si X from $3d \rightarrow 2p$ transitions.

Our sample consists of 5 stars including three normal dwarf stars, i.e., Procyon and α Cen A and B, an active late-type dwarf star, ϵ Eri, and an active binary system Capella. The properties of our sample, along with ObsID and exposure time are summarized in Table 1. All observations adopt grating of LETGS combined with HRC instrument on board *Chandra* Observatory. In case of Capella, an additional observation (with ObsID=55) with ACIS-S instrument is used. Because ACIS-S instrument has significant energy resolution to separate overlapping spectral orders, LETGS+ACIS-S observations are better choice for determination of the electron density. However only one observation is available from *Chandra Data Archival Center* for our sample. Another goal of analysis for the ACIS-S spectrum of Capella is to validate whether there is significant contamination from high-order (refer to $m \geq 2$) spectra around the selected lines (50.524 and 50.691 Å). If line fluxes derived from the two different observations are comparable, no contamination from high-order spectra can be concluded. This also backs up our analyses for other stars. Reduction of the LETGS datasets uses CIAO3.2 software with the science threads for LETGS/HRC-S observations. For the ACIS-S spectrum of Capella, **Destreak** tool was used to clean the events induced by detector artifacts on CCD 8 (“streaks”). For the extraction of the spectra of α Cen A&B, similar procedure as employed by Raassen et al. (2003) is adopted here under the CIAO environment. Figure 1 shows the spectra with background subtracted for Procyon, α Cen A&B, Capella and ϵ Eri in the wavelength range of 50–55 Å.

2.1. Determinations of line fluxes

The line fluxes were derived by modelling the spectrum locally with narrow Gaussian profiles, in which the instrumental effective area extracted from CIAO3.2 calibration files with `fullgarf` tool has been folded, together with a constant representing the background and (pseudo)continuum emissions which were determined in the line-free region (51–52 Å). Here, only the positive order spectra has been adopted because there is a plate gap around 52 Å for the negative spectra. The average instrumental FWHM of lines is about 0.06 Å for LETGS observations. The fluxes have been obtained after correction for the effective area. In the fitting, 1σ uncertainty is adopted to determine statistical errors for the line fluxes, and no wavelength correction has been used to the dispersion relation of the HRC-S/LETG. The error bars determined in this method are slightly underestimated due to the adopted functional forms of the line profiles, which introduce a certain of systematic errors. Table 2 shows the theoretical wavelengths and measured fluxes of the two prominent lines of Si X, together with results of Fe XVI lines detected in Capella and ϵ Eri stars. Since the centered wavelength for a given line is also a thawed parameter in the fitting, the best-fit result is different for the different stars, yet it is consistent with theoretical identification within 30mÅ. So only the theoretical wavelength is given for each emission line in this table.

2.1.1. Procyon, α Cen A&B

For normal stars such as Procyon and α Cen A&B, a detailed description has been presented by Raassen et al. (2002, 2003) and a conclusion that the coronal plasmas are dominated by plasmas with temperatures ranging 1–3 MK was obtained. α Cen A and B were firstly spectrally resolved from observation with LETGS instrument, a detailed description about it is presented by Raassen et al. (2003). In the long wavelength region > 30 Å, $3d \rightarrow 2p$ transitions of Si X at 50.524 Å and 50.691 Å are the prominent lines,

which ensures the correct measurements of line fluxes. In order to measure the fluxes of the two lines correctly, contamination from higher order spectral lines of high ionized Fe ions should be taken into account. Fortunately, emission from high charged Fe ions is either weak or absent in first order (and particularly in third order which is damped by a factor ≈ 20) for inactive stars. In addition, the temperature of peak emissivity of Fe XVI lines ranging this wavelength region is about 4 MK, which is higher than that of X-ray emitting plasma. Such that no emission lines of Fe XVI are detected for the three stars.

In order to obtain the line fluxes, two Gaussian profiles with the same FWHM value, combining with a constant were used in fitting the spectra in 50–51 Å. The continuum level is around $1.2 \times 10^{-4} \text{ photon s}^{-1} \text{ cm}^{-2} \text{ Å}^{-1}$ for the three normal stars, which is determined by fitting with a constant model in line-free wavelength region 51–52 Å. The best-fit values of line fluxes are listed in Table 2, along with statistic errors (with percentage) derived with 1σ uncertainty. The observed wavelengths are within 10 mÅ, when compared with experimental ones. The reduced χ^2 are 0.76, 0.63 and 0.67, respectively, which indicates present fitting is good for the three normal stars.

2.1.2. *Capella*

For active star Capella, numerous studies exist in the literatures for the active star Capella (Mewe et al. 2001, Canizares et al. 2000, Audard et al. 2001), which reported its properties using observations with different instruments. Most observations adopted this star as test platform to calibrate instruments on board satellites (Brinkmann et al. 2000). The observation adopting the ACIS-S instrument eliminates the contamination from high-order spectral lines for the selected lines (Si X). In order to validate whether there is contamination from the high-order spectral lines for the selected Si X lines, the observation with ACIS-S instrument is also analyzed. Here, the -1 order spectrum is adopted,

because no photon has been detected in +1 order spectrum above 30 Å. Nevertheless, the contamination from lines of Fe XVI around 50 Å is inevitable, since they have become the strongest lines as shown in Fig. 1. For much more active star, the emissions of Si X completely disappear.

In the fitting, four components (with same FWHM) combined with continuum emission ($5.7 \times 10^{-4} \text{ photon cm}^{-1} \text{ s}^{-1} \text{ Å}^{-1}$ determined in the line-free region) were used for the ACIS-S and HRC spectra in 50–51 Å. The reduced χ^2 for ACIS-S and HRC observations are 0.75 and 0.71, respectively. Fig. 2 shows the best-fit (dotted line) to the ACIS-S spectrum. In this plot, the HRC spectrum of Capella is also overlapped (dashed histogram) for the visual comparison though their effective areas are slightly different. The best-fit results of the two different observations indicate that there is no contamination from the high-order spectra. The derived line fluxes are comparable each other, such as for line at 50.367 Å, the derived fluxes are 2.38 ± 0.30 and $2.25 \pm 0.22 \times 10^{-4} \text{ phot.cm}^{-2} \text{ s}^{-1}$ for ACIS and HRC observations, respectively, for line at 50.691 Å, they are 0.98 ± 0.24 and $1.14 \pm 0.18 \times 10^{-4} \text{ phot.cm}^{-2} \text{ s}^{-1}$. Such consistency gives us confidence to use the line fluxes derived from HRC spectra for other stars, though no ACIS-S observation data is available for our sample. In case of Capella, ACIS-S spectrum was adopted for the analysis in the following.

In the spectra observed with ACIS-S and HRC, the line of Si X at 50.691 Å has been clearly detected. Is the observed flux at 50.576 Å completely from contribution of Si X at 50.524 Å? In the available database such as CHIANTI, MEKAL and APED, we note that Fe XVI line at 50.555 Å may also be the significant source of contribution to the observed flux at 50.576 Å, because present instrument can not resolve the two emission lines obviously. The most prominent lines at 50.367 Å, 54.136 Å and 54.716 Å in this range were identified to be emissions of Fe XVI by Raassen et al. (2002), which further confirms that Fe XVI contribute to the observed flux at 50.576 Å. So an another problem

is that how much fraction of the flux at 50.576 Å comes from Si X emission at 50.524 Å.

The emission measure distribution (EMD) of Capella has been derived from different observations with different instruments with high-resolutions such as HEG (Canizares et al. 2000), LETGS (Mewe et al. 2001) on board *Chandra* and RGS (Audard et al. 2001) on board *XMM-Newton*. Their results indicate that the EMD has a sharp peak around 7 MK, together with a smaller one grouping around 1.8 MK which is necessary to explain the detected O VII He-like triplet and C VI Ly α line. Argiroffi et al. (2003) investigated its variability during different phase, and found that the emission is compatible with a constant source. In this work, we adopt the EMD derived from RGS observation by Audard et al. (2001), with combination of emissivity of Fe XVI included in (Astrophysical Plasma Emission Code) APEC model to derive the contributions of Fe XVI lines. We found that Fe XVI line at 50.555 Å contributes $\sim 62\%$ to the total observed fluxes ($2.38 \pm 0.30 \times 10^4 \text{phot.cm}^{-2}\text{s}^{-1}$). The remaining flux at this wavelength should come from Si X line at 50.524 Å. Additionally, we notice that there is a shoulder around 50.576 Å. So we fit the spectrum again by adding an additional component. We initially set two artificial components around 50.57 Å. The best-fit (smooth solid line in Fig. 2) of the spectrum shows a better result than the fitting with four components (dotted line) by the visual inspection. The reduced χ^2 is also more close to unity which changes from 0.75 to 0.79. Though the obtained flux ($2.07 \pm 0.28 \times 10^4 \text{phot.cm}^{-2}\text{s}^{-1}$) of Fe XVI line at 50.576 Å is slightly higher than the theoretical prediction (1.65), the two values from different procedure are comparable. The line flux of Si X line at 50.524 Å listed in Table 2, is from the fitting procedure.

For the line flux at 50.367 Å we further note that about $\sim 73\%$ contribution comes from Fe XVI line at 50.350 Å. A search of APEC shows that the remaining flux may be from contribution of Fe XVII lines (50.342 Å and 50.361 Å) and Si X (50.333 Å,

50.336 Å and 50.359 Å). As the strongest lines of Si X at 50.524 Å appear to be weak in Capella, we suggest that the remaining flux of the observed flux at 50.367 Å is from emission lines of Fe XVII. Using the EMD model derived by Audard et al. (2001) and the emissivity of Fe XVII predicted by the APEC model, we predict the total fluxes of the four lines are about 0.68×10^{-4} photon $\text{cm}^{-2} \text{s}^{-1}$, which is consistent with the remaining flux (0.97×10^{-4} photon $\text{cm}^{-2} \text{s}^{-1}$) within statistical error.

2.1.3. ϵ Eri

The detailed analysis for Capella reveals that the contamination due to high-order spectral lines is negligible. However, the emission from Fe XVI lines must be taken into account. Four components and a constant value are used to fit the spectrum of ϵ Eri in wavelength range 50–51 Å. The continuum emission determined in the line-free region is 1.2×10^{-4} photon $\text{cm}^{-1} \text{s}^{-1} \text{Å}^{-1}$. The best-fit (reduced $\chi^2=0.62$) results of line fluxes are listed in Table 2, along with 1σ statistical error.

For the flux extraction of Si X line at 50.524 Å, the similar procedure as for Capella is applied to estimate the contribution of Fe XVI lines. Using the emissivity of Fe XVI extracted from APEC and normalization according to the isolated line at 54.134 Å, we estimate that the contributions of Fe XVI to the observed fluxes around 50.350 Å and 50.555 Å are about 53% and 39%, respectively. For line flux around 50.550 Å, the remaining flux is from contribution of Si X line (50.524 Å).

3. Theory model of line ratio

In our previous paper (Liang et al. 2005), we describe properties and application of Si X spectrum in detail, and found that six line ratios are sensitive to electron density. One of

these ratios R_1 has a good application on density diagnostic because the two lines are the strongest lines in the spectrum of collision dominated low-density plasma. For consistency, we describe the property of the ratio R_1 briefly, and the model considered in our calculation. The ratio R_1 is defined as

$$R_1 = \frac{I(\lambda 50.524 \text{ \AA})}{I(\lambda 50.691 \text{ \AA}) + I(\lambda 50.703 \text{ \AA})} \quad (1)$$

Radiative rates, and electron impact excitation as well as de-excitation among 320 levels of Si X have been included in the calculation of line intensities at the steady state condition for different electron densities. The energy level is replaced by experimental value if it is available. Excitation rates by protons of Foster, Keenan & Reid (1997) are also taken into account, which are calculated by using the close-coupled impact parameter method. In the observed spectra, the two lines (50.691 Å and 50.703 Å) are blended. So the sum of the intensities of these two lines is used in definition and calculation.

Figure 3 shows the ratio as a function of the electron density n_e at three different logarithmic electron temperature ($\log T_e(\text{K})$): 5.9, 6.1 and 6.3. The ratio is sensitive to the electron density in the range from 10^7 cm^{-3} to 10^{10} cm^{-3} which matches conditions that known to appear in various stellar object. The effect of electron temperature on the ratio appears to be important at a low-density limit $n_e < 5 \times 10^6 \text{ cm}^{-3}$, while the effect is negligible above $2 \times 10^8 \text{ cm}^{-3}$ as shown in Fig. 3. This is an important feature for density diagnostics. The line intensity at 50.703 Å holds the sensitivity to the electron temperature and density. At the high-density, it is negligible when compared with that of line at 50.691 Å, but it appears to be comparable at low-density limit. So the slight sensitivity to the electron temperature is present in the low-density region as shown in Fig. 3.

4. Results and discussions

4.1. Diagnostic of the electron density

Based on the measurements of line fluxes for individual lines of Si X, the observed line ratios are obtained for our sample, which are listed in Table 3. All these ratios are located in the density-sensitive range ($R_1 \sim 6$ – 2.7), so the electron density of X-ray emitting layer of stellar coronae can be derived. For Capella, the emission lines of Si X appear to be weak, and one feature (50.524 \AA) is strongly contaminated by emission line of Fe XVI as shown in sect.2, so the observed ratio shows a relatively large uncertainty.

By comparing observed ratios with the theoretical prediction, electron densities of stellar coronae are derived for our sample which are listed in Table 3. Figure 4 shows such comparison, in which the solid line is prediction at the logarithmic electron temperature 6.1 of maximum fraction of Si X in the ionization equilibrium of Mazzatto et al. (1998), symbols with errors are observed ratios of our sample. All the observed ratios are around unity within uncertainty, which result in that the diagnosed electron densities distribute in the range of 10^8 – 10^9 cm^{-3} . One component (α Cen B) of the binary α Centauri shows a same ratio with that of Procyon, while the other component shows a value close to that of ϵ Eri. Therefore the electron densities for the two stars share the same value as shown in Fig. 4. The work of Raassen et al. (2003) also indicates the similar properties between α Cen B and Procyon. The ratio between $Ly\alpha$ of H-like O VIII and resonance lines (or triplet) of He-like O VII for α Cen B is very close to that of Procyon (see top pannel of Fig. 9 in work of Raassen et al. (2003)).

4.2. Discussions

A systematic analyses of extreme ultraviolet spectra for 28 stellar coronae performed by Sanz-Forcada et al. (2003), reveals that the stellar coronae consistent with two basic classes of magnetic loops: solar-like loops with maximum temperature around $\log T_e(\text{K}) \sim 6.3$ and lower electron densities ($n_e \geq 10^9 - 10^{10.5} \text{cm}^{-3}$), and hotter loops peaking around $\log T_e(\text{K}) \sim 6.9$ with higher electron densities ($n_e \geq 10^{12} \text{cm}^{-3}$). For the hotter temperature region, the electron densities are usually derived from highly charged iron ions with higher peak temperature in the ionization equilibrium (Mazzotta et al. 1998). Sanz-Forcada et al. (2003) derived the electron densities are more than 10^{12}cm^{-3} from EUV spectra observed with EUVE satellite. An upper limit ($5 \times 10^{12} \text{cm}^{-3}$) for stellar coronae was concluded by Ness et al. (2004) from carbon-like iron lines with fluxes extracted from Low Energy Transmission Grating Spectrometer (LETGS) spectra. From resolved triplets of He-like magnesium and silicon, upper limits 7×10^{11} and $1 \times 10^{12} \text{cm}^{-3}$ for Capella were derived by Canizares et al. (2000) from the HEG spectra. Through de-blending the contamination for Ne IX triplet, Ness et al. (2003) place an upper limit of $2.0 \times 10^{10} \text{cm}^{-3}$ for Capella.

Ness et al. (2002, 2004) further made a detailed investigation for the coronal density using He-like triplet, and found that the derived densities from He-like C, N and O do not deviate from low-density limits for inactive stars. For the cool X-ray emitting region, O VII triplet is extensively used to derive the electron density for stellar coronae because of its high SNR around 21 \AA . Whereas the C V triplet forms at a much cooler emitting layer which should carry out information in this emitting layer. For inactive and some active stars, the C V triplet can be detected and the corresponding electron density has been published in literatures (Ness et al. 2001). In ionization equilibrium of Mazzotta et al. (1998) condition, the temperature (1.26 MK) of maximum fractional abundance of Si X is close to that derived from H- and He-like C. Therefore the electron densities from the two

approaches should be compatible with each other. Here we make a comparison between our results and the values constrained by Ness et al. (2001; 2002) for our sample, as shown in Fig. 5.

The figure reveals that our results are consistent with those of Ness et al. (2001, 2002) within 1σ statistical uncertainty, which suggests that electron densities derived from spectra of ions with similar formation temperature are compatible with each other. For three inactive stars, the density derived from the two methods shows an excellent agreement. The uncertainties of our results are much smaller than those constrained by He-like C V. The large uncertainty in the electron densities derived from He-like C V is due to a faint inter-combination line presented, which results in that the observed ratio i/f between the inter-combination (i) and forbidden (f) lines located near the low-density limit. The flux measurement for i line is strongly depended on the determination of continuum level, so a relatively larger uncertainty appears in constrained electron densities. For selected lines in this study, no faint emission lines are involved. The line fluxes of the two features are comparable for these inactive stars. The observed ratios are close to unity, which corresponds to the density-sensitive region. In case of α Cen A (G2V), only upper limit of density can be obtained from C V triplet because a faint inter-combination line is present. However present work further constrains the mean electron density for the cooler layer of the star.

In case of Capella, the derived electron density also agrees with that derived from C V, whereas our result shows a larger error bar. One reason is due to that the emission line of Si X at 50.524 Å is severely contaminated by line of Fe XVI at 50.555 Å. Another possible reason may be the determination of continuum level, because the emission lines of Si X have become weak for active stars. For ϵ Eri, the electron density is not available from C V because the forbidden line is severely contaminated. The electron density of $1.29 \times 10^9 \text{ cm}^{-3}$

constrained by Si X could be used to represent the density in C V forming region.

5. Conclusions

For inactive stars, such as Procyon and α Cen A and B, emission lines of Si X at 50.524 Å and 50.691 Å are the prominent lines with high SNR in the wavelength range 35–70 Å. Our previous paper indicates that the ratio R_1 between the two lines is sensitive to electron density, while it is insensitive to electron temperature. This is a good feature for diagnostic of the electron density for hot astrophysical and laboratory plasmas. In the low-density limit region, the obvious temperature effect of the ratio is due to contamination by $3d \rightarrow 2p$ transition of Si X at wavelength 50.703 Å. Compared with the intensity of line at 50.691 Å, the line intensity at 50.703 Å steeply decreases with increasing the electron density. In case of Capella, the line at 50.691 Å is clearly detected, while the line at 50.524 Å is severely contaminated by line of Fe XVI. Based on the conclusion of Argiroffi et al. (2003) that the emission of Capella is compatible with a constant source, we use the EMD derived by Audard et al. (2001) and line emissivity included in APEC1.3.1 model to estimate the contribution of Fe XVI line at 50.555 Å. About 62% flux is estimated to be from the contribution of Fe XVI, the remaining flux is from Si X line at 50.524 Å. The contribution of Fe XVI line at 50.367 is simultaneously estimated, which contributes about 73%. When the EMD is folded with emissivities of Fe XVII lines, the estimated flux of Fe XVII lines around 50.367 Å is 0.68×10^{-4} photon $\text{cm}^{-2} \text{s}^{-1}$ which is consistent with the remaining flux within statistical error. Applying the procedure to ϵ Eri, we conclude that the contributions of Fe XVI lines at 50.36 Å and 50.54 Å are about 53% and 39%, respectively. So the flux of Si X line at 50.524 Å is about 0.64×10^{-4} photon $\text{cm}^{-2} \text{s}^{-1}$.

The observed ratios of our sample are close to the unity which corresponds the density-sensitive range of R_1 . Comparison of our results with those derived from He-like

C V shows a good agreement. Moreover, the derived electron densities and error bars are similar for the inactive stars, but the error bars are large for the active stars. In conclusion, the emission lines of Si X have potential density-diagnostic application in stellar coronae and other X-ray sources.

This work was supported by the National Natural Science Foundation under Grant No. 10433010 and No. 10403007, as well as the Chinese Academy of Sciences under Grant No. KJCX2-W2.

REFERENCES

- Argiroffi, C., Maggio, A., & Peres, G., 2003, *A&A*, 404, 1033
- Audard, M., Behar, E., Güdel, M., et al. 2001, *A&A*, 365, L329
- Brinkmann, A. C., Gunsing, C. J. T., Kaastra, J. S., et al. 2000, *ApJ*, 530, L111
- Canizares, C. R., Huenemoerder, D. P., Davis, D. S., et al. 2000, *ApJ*, 539, L41
- Doyle, J. G. 1980, *A&A*, 87, 183
- Foster, V. J., Keenan, F. P., Reid, & R. H. G. 1997, *At. Data Nucl. Data Tables*, 67, 99
- Gabriel, A. H., Bely-Dubau, F., Faucher, P., et al. 1988, *J. Phys.*, 49, 235
- Güdel, M., Schmitt, J. H. M. M., Benz, A. O., et al. 1995, *A&A*, 301, 201
- Güdel, M., Audard, M., & Mewe, R. 2003, *A&A*, 403, 155
- Liang, G. Y., Zhao, G., Shi, J. R. 2005, *MNRAS*, 2005, (in referee)
- McKenzie, D. L., & Landecker, P. B. 1982, *ApJ*, 259, 372
- Mewe, R., Raassen, A. J. J., Drake, J. J., et al. 2001, *A&A*, 368, 888
- Ness, J. -U., Brickhouse, N. S., Drake, J. J., et al. 2003, *ApJ*, 598, 1277
- Ness, J. -U., Güdel, M., Schmitt, J. H. M. M., et al. 2004, 427, 667
- Ness, J. -U., Mewe, R., Schmitt, J. H. M. M., et al. 2001, *A&A*, 367, 282
- Ness, J. -U., Schmitt, J. H. M. M., Burwitz, V., et al. 2002, *A&A*, 394, 911
- Peres, G., Orlando, S., Reale, F., et al. 2004, *ApJ*, 612, 472
- Raassen, A. J. J., Mewe, R., Audard, M., et al. 2002, *A&A*, 389, 228

Raassen, A. J. J., Ness, J. -U., Mewe, R., et al. 2003, *A&A*, 400, 671

Sanz-Forcada, J., Brickhouse, N. S., Dupree, A. K. 2003, *ApJS*, 145, 147

Siarkowski, M., Pres, P., Drake, S. A., et al. 1996, *ApJ*, 473, 470

Scelsi, L., Maggio, A., Peres, G., et al. 2005, *A&A*, 432, 671

Schmitt, J. H., M. M., & Kürster, M. 1993, *Science*, 262, 215

Smith, R. K., Brickhouse, N. S., Liedahl D. A., et al. 2001, *ApJ*, 556, L91

Vaiana, J. S., et al. 1981, *ApJ*, 245, 163

White, N., E., Shafer, R., A., Parmar, A. N., et al. 1990, *ApJ*, 350, 776

Table 1: Summary of stellar properties and measurement of X-ray luminosity (in range of 5–175 Å) for the stars. t_{obs} denotes the exposure time of observations.

star	HD	ObsID	t_{obs}	Spectr.Type	distance ^a	T_{eff}^a	$\log(L_{bol})$	R_{\star}^a	L_X^b
			ks		pc	K	erg/s	$[R_{\odot}]$	10^{28} erg/s
Procyon	61421	63	69.6	F5.01V – V	3.5	6540	34.46	2.06	2.43
α Cen A	128620	29	79.5	G2.0V	1.34	5780	33.77	1.23	0.65
α Cen B	128621	29	79.5	K0.0V	1.34	5780	33.28	0.8	0.52
Capella	34029	1248	84.7	G1.0III/K0.0I	12.94	5850	35.71	9.2/13	255
ϵ Eri	22049	1869	105.3	K2.0V	3.22	4780	33.11	0.81	20.9

^aFrom Ness et al. (2004)

^bFrom Ness et al. (2002).

Table 2: Line fluxes (in unit of 10^{-4} photon $\text{cm}^{-2} \text{s}^{-1}$) of prominent lines in wavelength range 50–55 Å for stars: Procyon, α Cen A&B, Capella and ϵ Eri. The values in parentheses are the errors (in percent) with 1σ uncertainty.

Ions	λ_{theo} (Å)	Procyon	α Cen A	α Cen B	Capella	ϵ Eri
Fe XVI	50.350	–	–	–	4.01(37) ^a	1.31(15) ^a
Si X	50.524	1.68(15)	0.99(10)	0.89(12)	0.85(23) ^a	0.64(14) ^a
Fe XVI	50.555	–	–	–	2.07(28) ^a	0.40(14) ^a
Si X	50.691	1.30(14)	0.91(11)	0.78(10)	1.14(18)	0.77(13)
Fe XVI	54.142	–	–	–	2.57(40)	0.76(14)
Fe XVI	54.728	–	–	–	5.67(54)	1.33(16)

^a blended lines

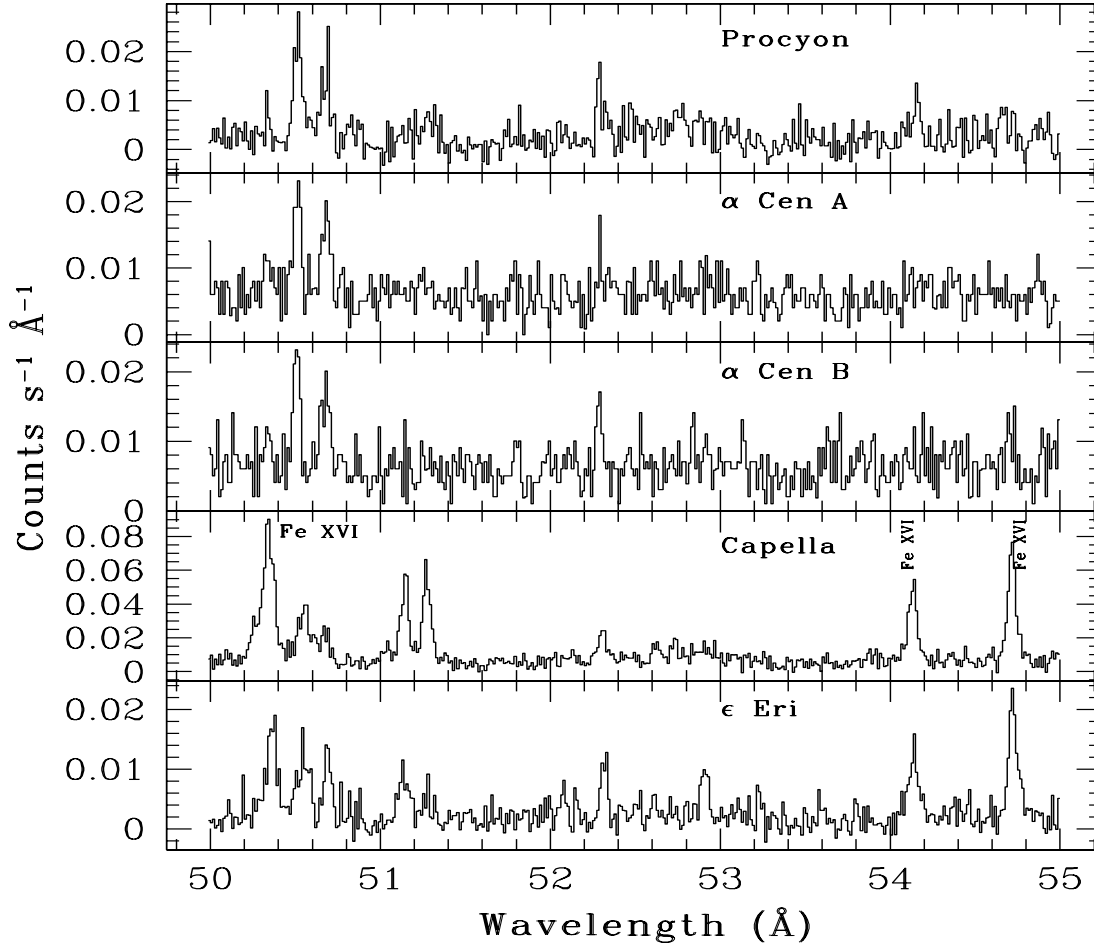


Fig. 1.— Extracted LETGS spectra of our sample in wavelength range 50–55 \AA . HRC-S instrument was used for all observations. In the fourth panel (from top), prominent lines from Fe XVI are labelled.

Table 3: Observed line intensity ratios for our sample, and diagnosed electron densities (in $\log n_e/\text{cm}^{-3}$), together with the statistic errors within 1σ .

	Procyon	α Cen A (G2V)	α Cen B (K1V)	Capella	ϵ Eri
Ratio	1.29 ± 0.25	1.09 ± 0.24	1.31 ± 0.39	0.73 ± 0.48	0.83 ± 0.32
$\log n_e$ (cm^{-3})	$8.61^{+0.24}_{-0.20}$	$8.81^{+0.27}_{-0.23}$	$8.60^{+0.39}_{-0.32}$	$9.30_{-0.48}$	$9.11^{+1.40}_{-0.38}$

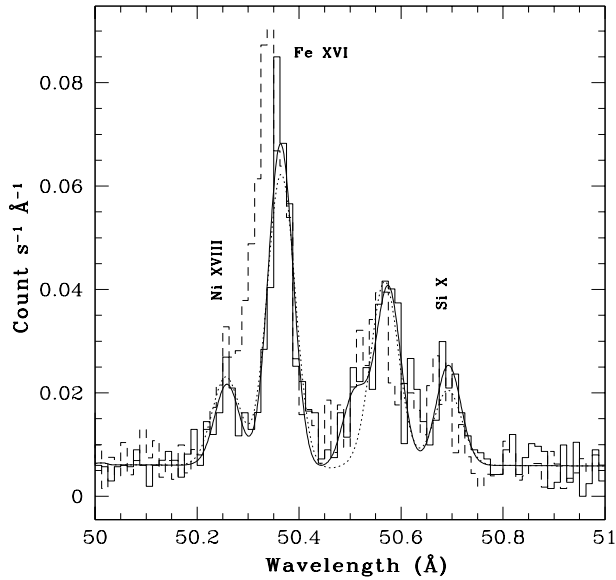


Fig. 2.— Spectra of Capella observed with ACIS-S (solid histogram) and HRC (dashed histogram) instruments in wavelength range 50—51 Å and best-fit spectra of ACIS-S spectrum with five (solid smooth line) and four (dotted line) Gaussian profiles, together with a constant representing background and (pseudo)continuum.

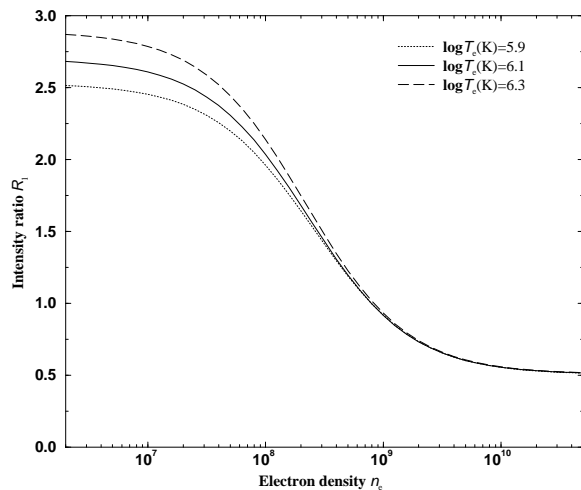


Fig. 3.— Line intensity ratio R_1 as a function of the electron density n_e at three different electron temperature ($\log T_e(\text{K})$): 5.9, 6.1 and 6.3.

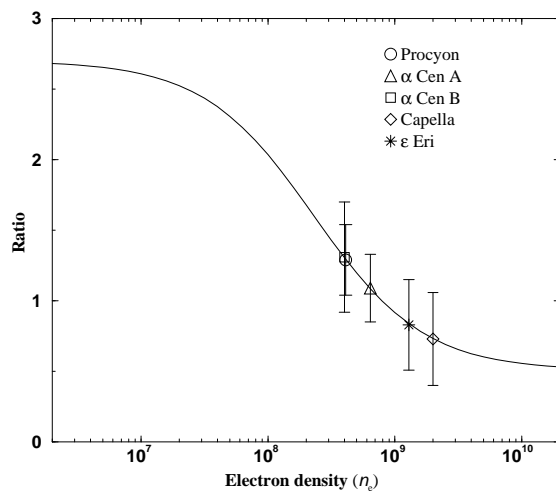


Fig. 4.— Observed line intensity ratio (symbols with 1σ error bars) for our sample and theoretical prediction at the logarithmic electron temperature $\log T_e(\text{K})=6.1$ (solid line).

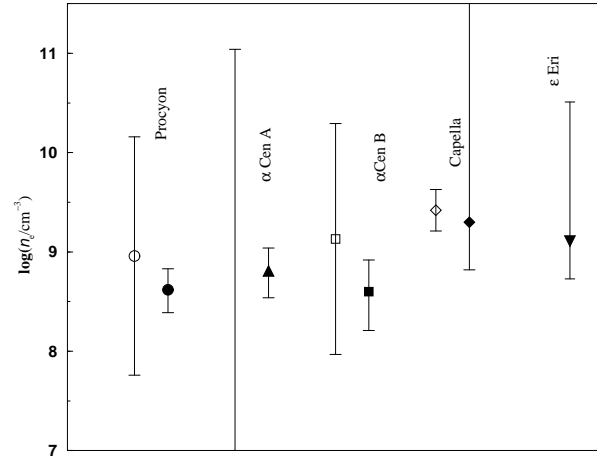


Fig. 5.— The electron density derived from ratio R_1 of Si X (filled symbols with errors) and from C V triplet (open symbols with errors).